Research Square

Preprints are preliminary reports that have not undergone peer review.
They should not be considered conclusive, used to inform clinical practice,
or referenced by the media as validated information.

Iontronic triboelectric tele-perception enabled by ion-relaxation engineering and a lightweight 1D-CNN decoder

Jiaxin Guo
Beijing Institute of Nanoenergy and Nanosystems
Yan Du
Beijing Institute of Nanoenergy and Nanosystems
Zhong Lin Wang
Beijing Institute of Nanoenergy and Nanosystems
Di Wei
weidi@binn.cas.cn

Beijing Institute of Nanoenergy and Nanosystems

Research Article

Keywords: Triboelectric tele-perception, Iontronic dielectric, Ionic relaxation, Waveform engineering, 1D convolutional neural network

Posted Date: November 20th, 2026

DOI: https://doi.org/10.21203/rs.3.rs-11588570/v1

License: This work is licensed under a Creative Commons Attribution 4.0 International License.
Read Full License

Additional Declarations: No competing interests reported.

Abstract

Robots must recognize what is approaching before they touch it. Triboelectric tele-perception meets this need, but its responses stay pinned to the material permittivity (dielectric constant) of the target: the voltage waveform collapses to a scaled copy of the electrostatic coupling, and material identity must then be recovered from a handful of amplitudes. We show that ionic relaxation in an iontronic dielectric breaks this constraint. Dispersing room temperature ionic liquid of BMIMTFSI (10 wt%) in thermoplastic polyurethane (TPU) gives an iontronic triboelectric sensor (ITS) whose mobile ions relax on the time scale of an approach event, so that ionic polarization and electrostatic induction act as two independent contributions to the same voltage transient. The resulting waveforms differ in shape, not merely in height: the iontronic film retains 91.57% of its initial output after 10^5 cycles and resolves four target materials as distinct polarity-amplitude classes at 70 mm. Because the discriminating information lies in the waveform morphology, a generic one-dimensional convolutional neural network (1D-CNN) fed with raw voltage traces classifies the four materials at 90.5% mean accuracy without hand-crafted features. We use this output to drive material-specific robot motions and a polarity-gated three-level warning display. Ionic relaxation thus supplies a design degree of freedom that is orthogonal to permittivity, and it turns an electrostatic proximity signal into a material fingerprint that a small decoder can read.

1 Introduction

Robots that work alongside people must decide what is approaching before contact[1, 2]. Tactile sensors learn the identity of an object only after they touch it, and therefore cannot withhold a motion in time[3–7]. Triboelectric tele-perception offers a way out: electrostatic induction converts an approaching charged object into a voltage transient while the object is still at a distance[8–12]. Existing platforms, however, read a single number from that transient. Their response scales with the permittivity of the target, so amplitude alone carries little material information, and the missing information is usually recovered with heavier computation[13–16].

Iontronic dielectrics change what the transient contains[17–19]. Mobile ions inside the sensing layer relax on the time scale of an approach event, and their redistribution adds a second, dispersive contribution to the electrostatic one[20–23]. The recorded voltage therefore acquires a material-dependent shape, and the information that amplitude alone could not provide becomes accessible in the waveform. A one-dimensional convolutional neural network (1D-CNN) can read this shape directly: it extracts local morphological features from raw traces and needs neither a temporal model nor hand-selected descriptors such as peak height[24–26].

Here we combine the two ideas in a tele-perception platform built on an iontronic triboelectric sensor (ITS) with a room temperature ionic liquid of BMIMTFSI-modified thermoplastic polyurethane (TPU) dielectric. We first establish how ionic loading, approach frequency, and separation distance govern the electrical output, demonstrating that 10 wt% BMIMTFSI maximizes the response while markedly improving cycling stability over 100,000 cycles compared with pristine TPU. We then show that the four

target materials fall into separable polarity–amplitude classes at 70 mm, and that a lightweight 1D-CNN trained on raw waveforms identifies them with 90.5% mean accuracy. Finally, we map the recognized class onto robot motions and onto a polarity-gated warning display. The results establish ionic relaxation as a modulation degree of freedom for triboelectric tele-perception, orthogonal to the electronic induction that conventional devices rely on.

2 Materials and methods

2.1 Materials and preparation of TPU/BMIMTFSI films

Thermoplastic polyurethane (TPU, grade 1185A) was purchased from BASF Polyurethanes. N,N-Dimethylformamide (DMF) served as the solvent, and 1-butyl-3-methylimidazolium bis(trifluoromethanesulfonyl)imide (BMIMTFSI) as the ionic liquid modifier.

TPU/BMIMTFSI composite films were prepared by solution casting. TPU was dissolved in DMF at a TPU-to-DMF mass ratio of 1:8 under continuous stirring at 80°C for 6 h. BMIMTFSI was then added at 5, 10, 15 or 20 wt% relative to the mass of TPU, and the mixtures were stirred at 60°C for 2 h. The solutions were cast onto aluminum foil and dried at 60°C for 2 h and then at 80°C for 10 h. Pristine TPU films were prepared by the same procedure without BMIMTFSI.

2.2 Fabrication and electrical characterization of the ITS

Square acrylic substrates (2.5 cm × 2.5 cm) were cut by laser and covered with copper (Cu) foil electrodes. The TPU/BMIMTFSI films were trimmed to the same dimensions and laminated onto the Cu electrodes to ensure intimate interfacial contact. The exposed electrode regions were insulated with electrical tape, and lead wires were connected to the Cu foil for signal acquisition. Devices incorporating pristine TPU and the different BMIMTFSI loadings were assembled in the same way.

Tele-perception characteristics were evaluated in the single-electrode configuration. A linear motor (LinMot S01-72/500) controlled the periodic approach and withdrawal of charged target materials. The open-circuit voltage was recorded with a programmable electrometer (Keithley 6514) connected to a National Instruments NI 6346 data acquisition (DAQ) card, and a custom LabVIEW program handled acquisition, processing and storage.

We examined the influence of BMIMTFSI concentration on the voltage response at a minimum sensor–target separation of 10 mm. Frequency-dependent measurements were performed at 0.5, 1, 2 and 3 Hz with a fixed displacement amplitude of 20 mm. Cycling durability was tested at 1 Hz and 10 mm separation over 100,000 approach-retraction cycles. Distance-dependent responses were characterized at separations from 5 to 80 mm. Material-dependent signals were recorded with FEP, PTFE, Fur and Nylon targets at 70 mm. Human proximity detection was performed at approximately 1.28 m under ambient conditions (25°C, ~ 38% relative humidity), with the device kept stationary and no additional conductive objects introduced into the sensing region.

2.3 Signal processing and material classification

Voltage waveforms from individual tele-perception events were collected for material classification. Four target materials (FEP, PTFE, Fur and Nylon) were investigated at a fixed separation of 70 mm. For each material we conducted 20 independent experimental groups with 10 repeated waveform measurements per group, yielding 800 samples in total. Training, validation and test sets were split at a ratio of 7:1:2 at the level of the experimental group to prevent data leakage between subsets. A 1D-CNN with three convolutional and max-pooling blocks, global average pooling and a fully connected classification layer extracted discriminative features from the voltage time series and assigned the four material classes.

2.4 Functional demonstrations

We built two functional demonstrations. A virtual humanoid robot interface was implemented in MATLAB (MathWorks, USA), in which four predefined motions—waving, arm swinging, nodding and arm raising—were assigned to FEP, PTFE, Fur and Nylon, respectively; the motion was triggered by manual material selection in the graphical interface. In parallel, a LabVIEW-based warning system monitored the sensor output and activated visual indicators against preset voltage thresholds: red for strong positive responses, yellow for weak positive responses and green for negative responses.

3 Results and discussion

3.1 Design and working principle of the tele-perception system

The platform combines a flexible TPU-based ITS modified with BMIMTFSI and a 1D-CNN decoder. The ITS comprises the iontronic dielectric as the functional sensing layer, a pair of electrodes and a supporting substrate. Its operation rests on electrostatic induction coupled to ionic relaxation inside the dielectric (Fig. 1). When a charged object approaches or recedes from the sensing surface, the surrounding electrostatic field is perturbed and the device delivers a measurable voltage without physical contact[8, 9]. Because the ions respond on their own time scale, the perturbation reaches the external circuit through two channels, and the resulting waveform, not just its amplitude, depends on the target.

The 1D-CNN reads this waveform directly. Raw voltage time series enter the network, which learns local features and assigns one of four classes: FEP, PTFE, Fur or Nylon. We then tested whether the recognized class can drive a response. An interactive humanoid demonstration linked each material to a predefined motion, and an automatic warning system translated the polarity and amplitude of the voltage into visual indicators. Together these demonstrations show that a material-resolved tele-perception signal can be used downstream without further signal conditioning.

3.2 Tele-perception performance of the BMIMTFSI-modified TPU films

Tele-perception requires responses that are both detectable and repeatable. We therefore varied the BMIMTFSI loading of the TPU films and measured the output of 2.5 × 2.5 cm² devices under contact–separation actuation at 1 Hz and 20 mm displacement. The voltage rises with ionic fraction, peaks at 10 wt% and falls at higher loadings (Fig. 2a). Two opposing effects explain this optimum: mobile ions strengthen the dielectric polarization of the film, whereas excess ionic content raises charge mobility and accelerates leakage[20, 21, 27]. We used the 10 wt% formulation in all subsequent tele-perception tests.

Approach frequency sets the pulse repetition rate but leaves the response amplitude almost unchanged. Sweeping the frequency from 0.5 to 3 Hz shifted the pulse rate while the peak voltage stayed near − 6.5 V (Fig. 2b), which indicates that the signal magnitude is governed by the electrostatic boundary conditions of the sensing event rather than by the speed of approach. Cycling stability separates the two compositions more clearly (Fig. 2c). After 100,000 cycles the modified film retained 91.57% of its initial voltage, whereas pristine TPU retained 70.23%, so ionic liquid modification substantially improves signal stability during prolonged operation.

Sensing range is set by the decay of electrostatic coupling between the charged target and the sensing electrode. The induced voltage fell progressively as the target receded (Fig. 2d), and the 10 wt% film produced a stronger response than the other compositions at every separation tested, which is the practical benefit of ionic doping for weak-signal capture. The same device registered human motion at a distance of about 1.28 m (Fig. 2e). The platform therefore covers the distance range relevant to pre-contact robotic perception.

Beyond proximity alerting, the device resolves which material is approaching. At 70 mm, FEP and PTFE produced negative voltage responses and Fur and Nylon produced positive ones (Fig. 2f), so polarity separates the four materials into two classes; within each class, signal amplitude separates the pair. Polarity and amplitude together thus form an electrical fingerprint for each tested material, which is the information the decoder exploits.

3.3 1D-CNN recognition of material-dependent voltage time series

Material-specific waveforms set the basis for discrimination; the remaining task is to read them automatically. Each voltage time series enters three successive convolutional layers with 128, 128 and 256 filters (Fig. 3a). These layers extract hierarchical representations of the signal, and the following max-pooling operations reduce dimensionality while retaining prominent local responses. Global average pooling condenses the feature maps into a 256-dimensional vector, which a fully connected layer maps

onto the four classes. The network therefore learns what distinguishes the materials instead of relying on predefined voltage thresholds[28].

The learned features separate the four materials (Fig. 3b). Their clusters are distinct and compact, with limited overlap, which shows that the electrical responses carry separable material information. The arrangement of the clusters is consistent with the polarity and amplitude differences measured experimentally, so the network recovers the physical structure of the signal rather than an arbitrary partition.

Accuracy is balanced across the four classes (Fig. 3c). FEP, PTFE, Fur and Nylon are recognized at 90%, 92%, 90% and 90% respectively, giving a mean accuracy of 90.5%. Residual errors occur between material pairs that share a voltage polarity and have similar response amplitudes, most notably Fur and Nylon. Iontronic waveform shaping combined with 1D-CNN decoding therefore supports automated tele-perception material recognition, and it provides the computational link to the material-dependent feedback demonstrated below.

3.4 Intelligent action feedback and automatic warning

Two proof-of-concept modules translate recognition into action (Fig. 4). The action-feedback module maps an identified material class onto a predefined robot movement, and the warning module converts the voltage signature into an automatically triggered visual alert.

In the action-feedback module (Fig. 4a), each of the four material classes drives a separate robot behavior, and the simulation is fed with real sensing data acquired at a target–sensor distance of 70 mm. FEP triggers waving, PTFE arm swinging, Fur nodding and Nylon arm raising. Once the class is assigned to the measured waveform, the corresponding motion sequence runs, so the robot executes a distinct action for each detected material. The material-to-action mapping shows how a discrimination output can be interfaced with robotic control.

The warning system runs as a LabVIEW program that correlates measured voltage signatures with three discrete visual states (Fig. 4b). Signal polarity separates positive from negative responses, and the amplitude of positive responses subdivides that regime: a strong positive signal (~ 0.22 V) triggers red, a weaker positive signal (~ 0.14 V) triggers yellow and a negative signal (~ − 0.20 V) triggers green. The matching indicator activates as soon as the measured voltage crosses its preset threshold, which gives real-time visual feedback of the electrostatic signal generated by the approaching object.

4 Conclusion

We have built a flexible tele-perception platform in which a BMIMTFSI-modified TPU iontronic dielectric supplies the sensing function and a lightweight 1D-CNN supplies the decoding, and we have used it to discriminate materials before contact. Mobile ions add ionic relaxation to electrostatic induction, which reshapes the voltage waveform and enriches the material signature beyond what permittivity alone

allows. The optimized device retains 91.57% of its initial voltage after 100,000 cycles, and the four target materials yield distinct polarity, amplitude and waveform features that a 1D-CNN classifies at 90.5% mean accuracy. Mapping these classes onto robot motions and onto a polarity-gated warning display demonstrates an end-to-end path from iontronic electrostatic sensing to material-aware feedback. The main open questions are how the ionic relaxation time should be matched to the duration of an approach event, and whether a decoder trained on four laboratory materials transfers to the open set of objects a robot meets in practice. Ionic relaxation nevertheless gives triboelectric tele-perception a tuning parameter independent of the target, and it offers a route to material-aware interfaces for intelligent robotic systems.

Declarations

Ethics approval and consent to participate

All experiments involving human participants were conducted in accordance with relevant institutional guidelines and regulations. The experimental protocols were approved by the Committee on Ethics of Beijing Institute of Nanoenergy and Nanosystems (Approval No. H-2024038). The human-proximity detection experiments were performed by one of the authors, who was fully informed of the experimental purpose and procedures and voluntarily participated in the study. Informed consent was obtained from the participating author prior to the experiments.

Consent for publication

Not applicable.

Competing interests

The authors declare no competing interests.

Funding

This work was supported by the National Natural Science Foundation (grant number 22479016).

Author Contribution

D.W. and Z.L.W. proposed the idea and the project. D.W. supervised the whole project. J.X.G. and Y.D. designed all the experiments and carried out the experiments in this paper and analyzed the corresponding data. All the authors discussed the results and commented on the manuscript. D.W. and J.X.G wrote this paper. †J.X.G. and Y.D. contributed equally to this work.

Data availability

Data will be made available on request.

References

1. Yu K, Yi J, Wang J, Luo Q, Liu T, Liu Z, Gao F, Cui H, Bai Y, Liu Y, et al. Triboelectric Tactile Sensors for Embodied Intelligence: Design, Performances, and Applications. Adv Mater. 2026;38(59):e74599.
2. Du Y, Chu D, Amaratunga G, Wei D. Triboelectric Tactile Sens Intell Syst SmartSys. 2026;2(2):e70023.
3. Kappassov Z, Corrales J-A, Perdereau V. Tactile sensing in dexterous robot hands — Review. Robot Auton Syst. 2015;74:195–220.
4. Qu X, Liu Z, Tan P, Wang C, Liu Y, Feng H, Luo D, Li Z, Wang ZL. Artificial tactile perception smart finger for material identification based on triboelectric sensing. Sci Adv. 2022;8(31):eabq2521.
5. Song Z, Yin J, Wang Z, Lu C, Yang Z, Zhao Z, Lin Z, Wang J, Wu C, Cheng J, et al. A flexible triboelectric tactile sensor for simultaneous material and texture recognition. Nano Energy. 2022;93:106798.
6. Xie Y, Cheng H, Yuan C, Zheng L, Peng Z, Meng B. Deep learning-assisted object recognition with hybrid triboelectric-capacitive tactile sensor. Microsystems Nanoengineering. 2024;10(1):165.
7. Jia M, Guo D, Guo P, Pan J, Liu X, Ren L, Chi M, Wang Y, Tian S, Yang Z et al. Multimodal Piezotronic-Gated Ferroelectric Tunneling Junctions for High-Resolution Tactile Imaging. SmartSys. 2026;2(3):e70041.
8. Fan F-R, Tian Z-Q, Lin Wang Z. Flexible triboelectric generator. Nano Energy. 2012;1(2):328–34.
9. Du Y, Wang ZL, Wei D. Emerging sensing systems based on triboelectric nanogenerator. Nano Energy. 2025;143:111292.
10. Rong X, Zhao J, Guo H, Zhen G, Yu J, Zhang C, Dong G. Material Recognition Sensor Array by Electrostatic Induction and Triboelectric Effects. Adv Mater Technol. 2020;5(9):2000641.
11. Luo L, Lu C, Yin X, Jin T, Zhang QA, Non-Contact. Triboelectric Sensing System and Its Application in Material Identification. In 2024 *5th International Conference on Artificial Intelligence and Electromechanical Automation (AIEA)*, 14–16 June 2024, 2024; pp 200–205. https://doi.org/10.1109/AIEA62095.2024.10692380
12. Jin C, Zhang C, Yan P, Jiang M, Yin R, Li K, Zhao W, Bai Z. A Superhuman Sensing Triboelectric Nanogenerator with Boosted Power Density and Durability via a Bio-Inspired Janus Structure. Adv Funct Mater. 2024;34(37):2402233.
13. Du Y, Shen P, Liu H, Zhang Z, Yang F, Chu D, Ren T, Wang ZL, Wei D. Meta-structured electret heterointerface for resilient and adaptive tele-perception in embodied intelligence. Matter. 2025;8(12):102363.
14. Du Y, Shen P, Liu H, Zhang Y, Jia L, Pu X, Yang F, Ren T, Chu D, Wang ZL, et al. Multi-receptor skin with highly sensitive tele-perception somatosensory. Sci Adv. 2024;10(37):eadp8681.
15. Guo J, Du Y, Wang ZL, Wei D. A paradigm shift from traditional non-contact sensors to tele-perception. J Mater Chem A. 2025;13(13):8939–67.

16. Wang T, Xu K, Zhao E, Min G, Wicklein B, Tsamis C, Huang C, Konghuayrob P, Tang W. Unique Advantages of Triboelectric Nanogenerators for Wearable and Implantable Electronics. SmartSys. 2026;2(3):e70039.
17. Chang Y, Wang L, Li R, Zhang Z, Wang Q, Yang J, Guo CF, Pan T. First Decade of Interfacial Iontronic Sensing: From Droplet Sensors to Artificial Skins. Adv Mater. 2021;33(7):2003464.
18. Bai N, Wang L, Wang Q, Deng J, Wang Y, Lu P, Huang J, Li G, Zhang Y, Yang J, et al. Graded intrafillable architecture-based iontronic pressure sensor with ultra-broad-range high sensitivity. Nat Commun. 2020;11(1):209.
19. Li X, Wang ZL, Wei D. Iontronic logic control driven by dynamic electrical double layer regulation. Iontronics. 2025;1(1):2.
20. Gbadam GS, Park H, Lee C, Joo H, Gwak S, Yoon H-J, Ryu H, Lee SM, Lee JH, Lee J-H. Direct current generation in triboelectric nanogenerators through ionic dynamics and electrode polarization effects. Nat Commun. 2025;16(1):9540.
21. Wang B, Zhao H, Jin C, Xu Y, Ding W. Ionic-electrostatic modeling of solid-liquid triboelectric nanogenerators. Iontronics. 2026;2(2):17.
22. Han JH, Kim SY, Moon HC. Unveiling the Impact of Tailoring Ionic Conductor Characteristics on the Performance of Wearable Triboelectric Nanogenerators. ACS Appl Mater Interfaces. 2024;16(21):27778–84.
23. Du G, Shao Y, Luo B, Liu T, Zhao J, Qin Y, Wang J, Zhang S, Chi M, Gao C, et al. Compliant Iontronic Triboelectric Gels with Phase-Locked Structure Enabled by Competitive Hydrogen Bonding. Nano-Micro Lett. 2024;16(1):170.
24. Ismail Fawaz H, Forestier G, Weber J, Idoumghar L, Muller P-A. Deep learning for time series classification: a review. Data Min Knowl Disc. 2019;33(4):917–63.
25. Wang Z, Yan W, Oates T. Time series classification from scratch with deep neural networks: A strong baseline. In. 2017 *International Joint Conference on Neural Networks (IJCNN)*, 14–19 May 2017, 2017; pp 1578–1585. https://doi.org/10.1109/IJCNN.2017.7966039
26. Li R, Wei D, Wang ZL. Synergizing Machine Learning Algorithm with Triboelectric Nanogenerators for Advanced Self-Powered Sensing Systems. Nanomaterials. 2024;14(2):165.
27. Zhou Q, Zheng Y, Kinoshita K, Ikuno T. Effect of adding ionic liquid into polydimethylsiloxane on the output performance of triboelectric nanogenerator. Jpn J Appl Phys. 2024;63(12):121004.
28. Shen C, Chen J, Liu Y, Chen Z, Huang J. Triboelectric signal enhancement via interface structural design and integrated with deep learning for real-time online material recognition. Chem Eng J. 2024;500:156874.

Figures

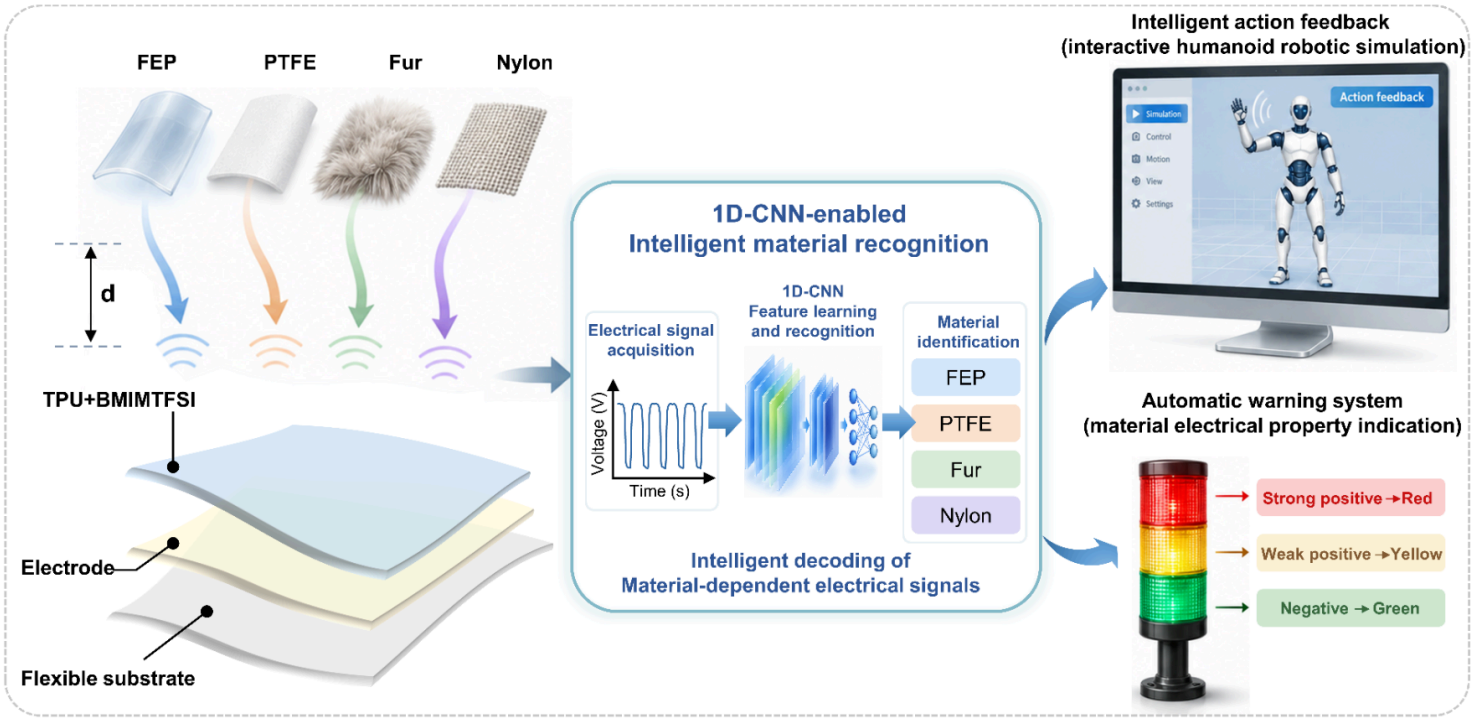

Figure 1

Ion-relaxation engineering and 1D-CNN decoding in a triboelectric tele-perception platform. An approaching charged object perturbs the electrostatic field of the iontronic dielectric; mobile ions relax on the time scale of the event and reshape the voltage transient. The recorded waveform is decoded by a 1D-CNN into a material class, which in turn drives robot actions and a visual warning display.

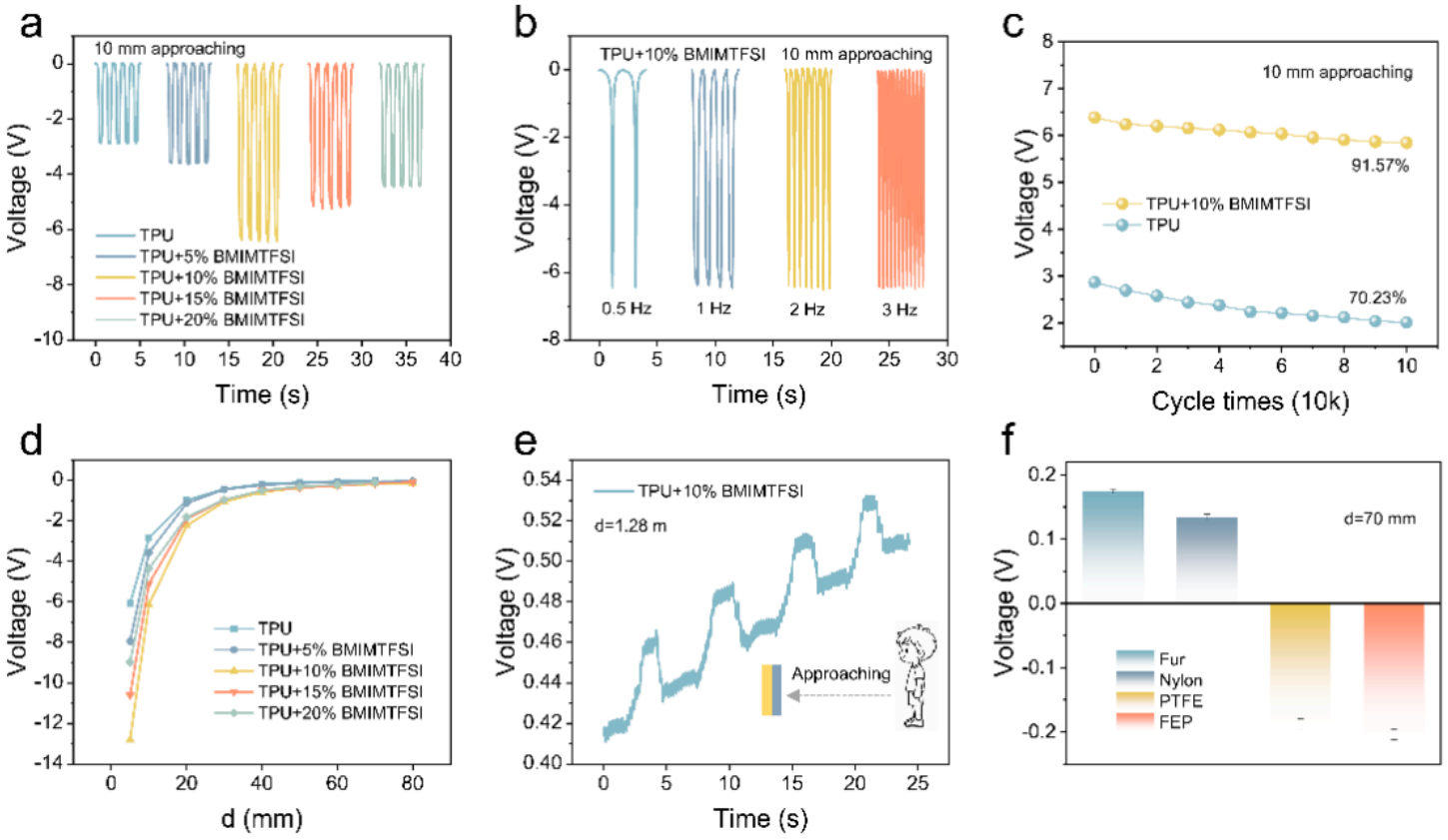

Figure 2

Electrical characteristics and tele-perception performance of BMIMTFSI-modified TPU films. (a) Output voltage of TPU films with different BMIMTFSI concentrations at an approach distance of 10 mm. (b) Voltage responses of the 10 wt% film at approach frequencies of 0.5–3 Hz; peak amplitudes remain nearly constant. (c) Cycling durability of pristine TPU and 10 wt% BMIMTFSI-modified TPU films over 100,000 cycles. (d) Output voltage versus separation distance for films with different BMIMTFSI concentrations. (e) Voltage response of the 10 wt% film to human approach at approximately 1.28 m. (f) Voltage polarity and amplitude for FEP, PTFE, Fur and Nylon targets at a sensing distance of 70 mm.

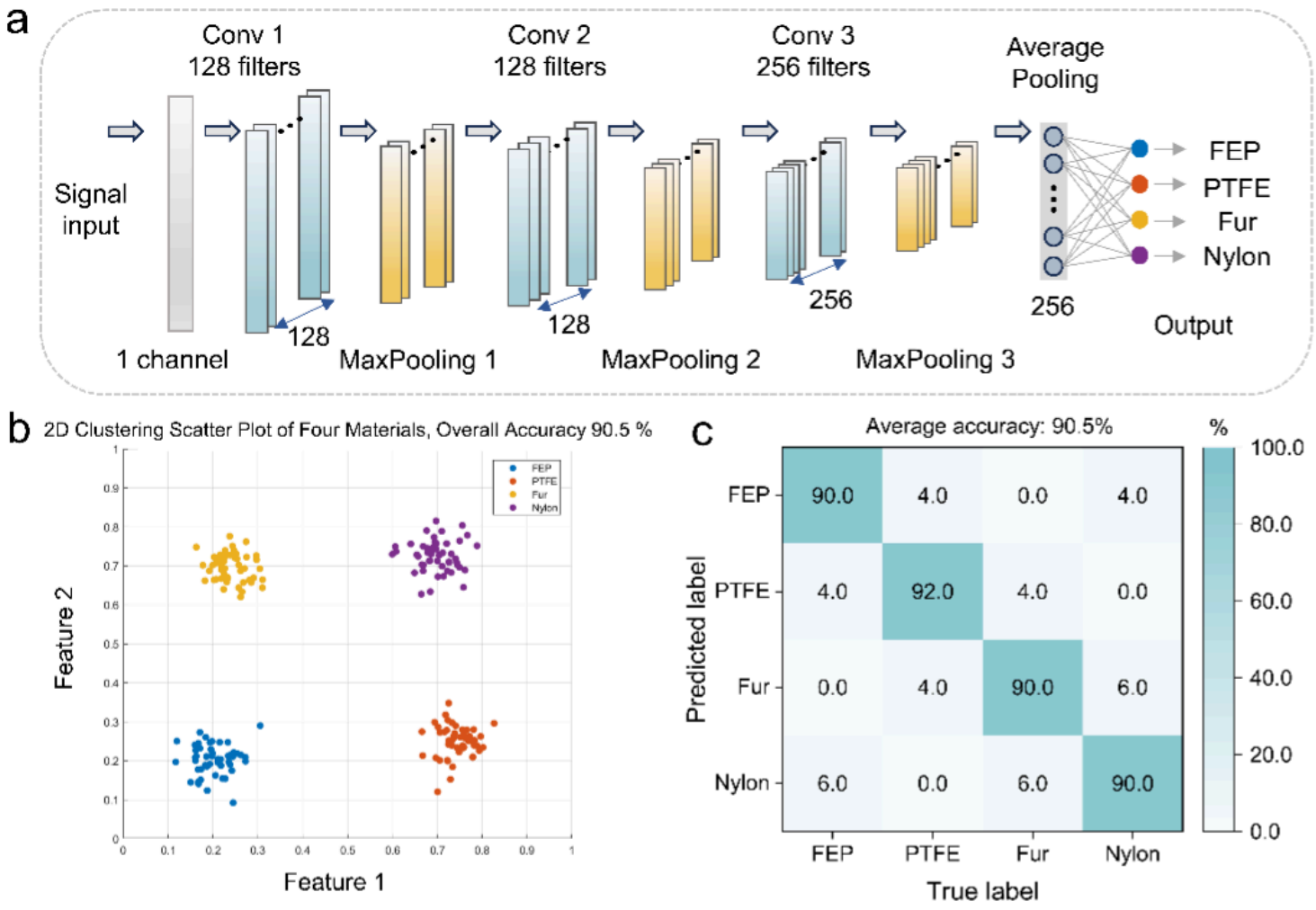

Figure 3

1D-CNN recognition of material-dependent voltage signals for pre-perception material identification. (a) Architecture of the 1D-CNN: three convolutional layers with 128, 128 and 256 filters, followed by max-pooling and global average pooling for four-class classification. (b) Two-dimensional feature distribution of the voltage signals from FEP, PTFE, Fur and Nylon. (c) Confusion matrix for the four materials, with a mean recognition accuracy of 90.5%.

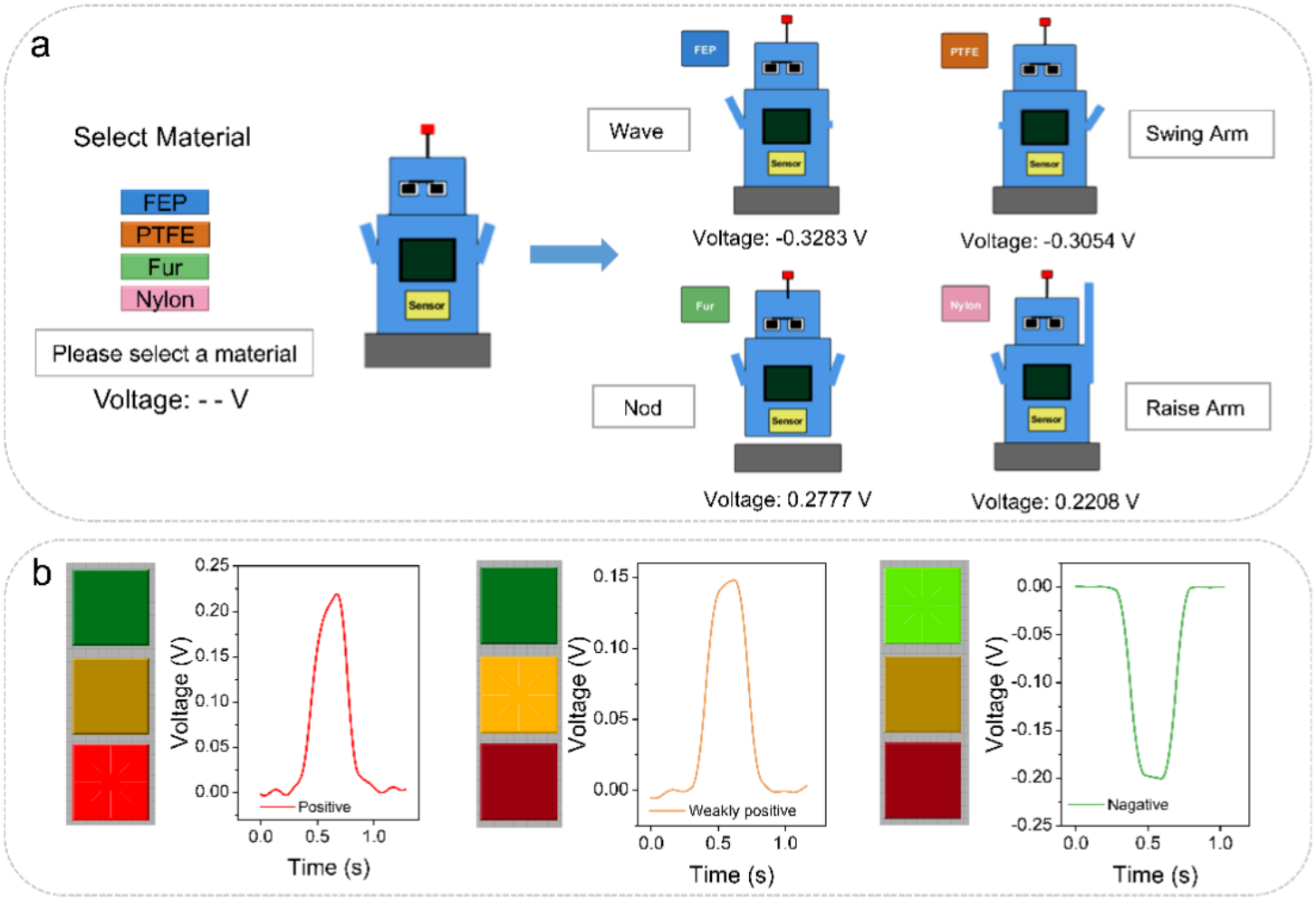

Figure 4

Functional demonstrations of the 1D-CNN-assisted tele-perception platform. (a) Intelligent action feedback: an interactive humanoid robotic simulation driven by the recognized material class. (b) Automatic warning system: material electrical properties indicated by a three-level visual display.